Biosensors and Bioelectronics 142 (2019) 111492

Contents lists available at ScienceDirect

Biosensors and Bioelectronics

journal homepage: www.elsevier.com/locate/bios

Protein recognition by polydopamine-based molecularly imprinted hollow spheres

Wei Chen*, Min Fu, Xixi Zhu, Qingyun Liu**

College of Chemical and Environmental Engineering, Shandong University of Science and Technology, Qingdao, Shandong, 266590, China

ARTICLE INFO

Keywords:
Surface imprinting
Protein recognition
Polydopamine
Hollow spheres

ABSTRACT

A facile method to prepare hollow molecularly imprinted polymers (HMIPs) for specific recognition of horseradish peroxidase (HRP) from biological samples was proposed in this paper. The HMIPs was prepared using silica nanoparticles as the sacrificial matrix and dopamine as functional monomer. The thickness of polydopamine shells can be easily modulated by tuning the mass ratio of silica matrix and dopamine. The polymerization conditions and recognition behaviors of the HMIPs were investigated systematically. The results suggested that the hollow structure endowed the HMIPs with fast adsorption kinetics of 25 min, high binding capacity of 172.1 mg/g, and reusability of no less than four adsorption-regeneration cycles without apparent deterioration. Meanwhile, excellent binding specificity towards HRP was presented in the selectivity studies. Moreover, enriching of HRP from human serum sample by the obtained HMIPs was conducted. The HMIPs displayed satisfactory binding specificity to HRP, in spite of the complex composition of the human serum.

1. Introduction

The specific recognition and efficient separation of target protein is extremely important in the field of clinical diagnostics and proteomics. Natural receptors with excellent specificity and binding affinity to their target molecules, have aroused great concerns. However, natural receptors usually suffer from poor physical/mechanical stability, cost inefficiency and complicated preparation process (Eersels et al., 2016). Therefore, increasing efforts have been devoted to synthesize artificial receptors for identification of the target molecules in specificity during the past decades (H. Bagheri et al., 2016a,b; Nakata et al., 2004; Qiu et al., 2018). To date, molecular imprinting has been identified as the most efficient and promising approach for the preparation of polymeric artificial receptors (Pan et al., 2018).

Molecularly imprinted polymers (MIPs) are generally synthesized by copolymerizing proper monomers and cross-linkers in the presence of template molecules. Followed by polymerization and removal of the imprinted molecules, recognition sites which are complementary chemically and sterically to the target molecules are obtained (Johari-Ahar et al., 2018; Pan et al., 2017; Zeinali et al., 2018). Compared with natural receptors, MIPs offer the advantages of low cost, good mechanical and chemical stability et al.(Kryscio and Peppas, 2012) To date, the imprinting of small molecules such as sugars (Xing et al., 2017), estrogen (Lucci et al., 2011), drugs (Bagheri et al., 2015; Munawar et al., 2018), pesticides (Saylan et al., 2017), and amino acid derivatives (Nishino et al., 2006) have been well achieved, and tailor-made MIPs are widely used in the areas of separations, artificial enzymes, chemical sensors, and pharmaceuticals (Dabrowski et al., 2018). Nonetheless, the imprinting of proteins and other biomacromolecules is still challenging owing to the complex spatial structure, huge dimension and changeful conformation of the macromolecular template. Various strategies have been proposed to achieve efficient protein imprinting, including metal coordination, surface imprinting, epitope imprinting and particle-based imprinting (Uzun and Turner, 2016). Among these methods, the surface imprinting turns out to be the most efficient one. The relatively thin polymer layer created by surface imprinting allows the location of the imprinted sites close to the surface of the MIPs, thus promoting the template molecules nearly complete removal and easy access to the binding sites (Kryscio and Peppas, 2012). Recently, the combination of surface imprinting with sacrificial support matrix to synthesize hollow MIPs has attracted increasingly attentions (Lu and Xu, 2017; Wang et al., 2016). The hollow structure can improve the binding capacity and mass transfer rate of the MIPs owing to the large surface area and low mass-transport resistance. For instance, Guan et al. reported imprinted single-hole hollow microspheres using 2,4,6,-trinitro-toluene as the template. The result demonstrated that the

* Corresponding author.
** Corresponding author.
E-mail addresses: chenwei30012@163.com (W. Chen), qyliusdu@163.com (Q. Liu).

https://doi.org/10.1016/j.bios.2019.111492
Received 12 April 2019; Received in revised form 30 June 2019; Accepted 3 July 2019
Available online 05 July 2019
0956-5663/

imprinted sites on the interior surface play important role on enhancing the rebinding ability of the imprinted hollow spheres(Guan et al., 2007). Chen et al. prepared lysozyme imprinted hollow spheres using silica particles as the support. The hollow imprinted polymers with extremely high binding capacity and selectivity were used to separate lysozyme from egg white successfully (Chen et al., 2013). In another report, hollow surface molecular imprinted polymer for rapid and selective recognition of dibenzothiophene was synthesized using porous magnetic carbon microspheres as the sacrificial support matrix (Hua et al., 2018). All those hollow MIPs exhibited satisfactory binding capacity and mass transfer rate to the template molecules. However, the effect of the imprinted layer thickness on the binding properties of the hollow MIPs was rarely studied.

Dopamine (DA), a biomolecule containing catechol and amine functional groups, has become a commendable monomer for protein imprinting. DA can be self-polymerized onto various substrates in a weak alkaline aqueous solution forming a hydrophilic and biocompatible polydopamine film. The polydopamine possesses plenty of non-covalent functionalities, which constructs multiple interactions with the target protein. Moreover, the thickness of the polydopamine film can be tuned by changing the mass ratio of the matrix material and the dopamine (Liu et al., 2014; Zhang et al., 2012).

Herein, a facile method was proposed to synthesize hollow molecularly imprinted polymers (HMIPs), using dopamine as functional monomer and silica nanospheres as the sacrificial matrix. In order to obtain HMIPs with excellent binding ability and specificity for target protein, the thickness of the HMIPs, the appropriate template protein amount and the polymerization time was investigated. Afterwards, the binding properties of the obtained HMIPs were evaluated by analysing the adsorption kinetics and the adsorption isotherms. Finally, the specificity of the HMIPs was verified by selective adsorption experiment and enrichment of the template protein from human serum samples.

2. Material and methods

2.1. Material

Tetraethyl orthosilicate (TEOS), dopamine hydrochloride, (3-Aminopropyl) and triethoxysilane (APTES) were bought from Sigma-Aldrich. Ethanol, toluene and ammonia solution (25–28%) were purchased from Chengdu kelong Chemical Reagent Co., Ltd. Horseradish peroxidase (HRP), bovine serum albumin (BSA), bovine hemoglobin (Hb), cytochrome C (Cyt C), ovalbumin (OVA) and lysozyme (Lys) were all purchased from Shanghai Aladdin Bio-Chem Technology Co., Ltd.

2.2. Instrumentation

Fourier Transform infrared spectroscopy (FTIR) measurement was carried out on a FTIR spectrometer (Nicolet 380 FT-IR). UV–vis spectroscopy measurement was carried out on a TU-1810 spectrophotometer. Scanning electron microscopy (SEM) measurements were carried out using an APREO. Transmission electron microscopy (TEM) was carried out on a JEM-2100 microscope.

2.3. Preparation of silica nanospheres

Monodispersed silica nanospheres were synthetized according to the Stöber method (Chen et al., 2017). In a typical procedure, ammonium hydroxide (30.0 mL), ultrapure water (70.5 mL) and ethanol (48.0 mL) were added into a one-neck flask, and stirred at a speed of 250 rpm. A mixture of tetraethoxysilane (TEOS, 13.5 mL) and ethanol (136.5 mL) was added into the flask. After stirring for 2 h at ambient temperature, the reaction solution was centrifuged at 10000 rpm, the obtained silica spheres were washed with ethanol and water three times, respectively. Finally, the obtained samples were dried in oven overnight at 45 °C.

2.4. Preparation of hollow molecularly imprinted polymers

The silica spheres (1 g) were dispersed in 80 mL toluene in a 250 mL flask under magnetic stirring. The SiO_2 in toluene were heated to 90 °C before adding APTES and toluene mixture, which helped to accelerate the diffusion of APTES in the mixture, further improving the homogenous modification of SiO_2. A mixture of 2 mL APTES in 20 mL toluene was added slowly by a dropping funnel. The mixture solution was continually stirred at 90 °C for 12 h. The modified nanospheres (SiO_2@NH_2) were collected and washed with acetone and ethanol several times.

For the preparation of hollow molecularly imprinted polymers, 200 mg SiO_2@NH_2 and 40 mg HRP were dispersed into 100 mL Tris buffer (10 mM, pH 8.0), and shaken for 3 h under ordinary temperature. Hence, HRP were oriented on SiO_2@NH_2 through forming multi-hydrogen bonds interaction between amino groups and carboxyl group in protein. After adding 200 mg dopamine, the mixture was stirred in an open beaker at room temperature for 9 h. Then, the polydopamine shell was coated on the HRP-binded silica nanospheres surface. Finally, to remove the silica matrix, the HRP-imprinted silica nanoparticles were washed with 2% hydrofluoric acid. Then, 20% acetic acid was used to remove the template protein, until no adsorption was detected by UV–vis spectrophotometer at about 280 nm(Hao et al., 2016). Hollow molecularly imprinted polymers (HMIPs) with binding sites corresponding to HRP were obtained. Similarly, the hollow non-imprinted polymers (HNIPs) were synthesized without adding HRP. The solid molecularly imprinted polymers (SMIPs) and solid non-molecularly imprinted polymers (SNIPs) were prepared in the same manner without removing the silica matrix.

2.5. Adsorption experiment

2.5.1. Static adsorption experiment

The static adsorption experiments were performed to evaluate the adsorption characteristics of the HMIPs and HNIPs. The detailed procedure is described as follows: 10 mg of the HMIPs was incubated with 3 mL HRP solutions (0.05–1.5 mg/mL) for 30 min. Afterwards, the HMIPs were separated by centrifugation. The concentration of unbinded HRP was determined by UV spectrometer. And the adsorption capacity (Q) of the HMIPs for HRP was figured out by formula (1)(Pang et al., 2006):

$$Q = (C_0 - C_f)V/m \quad (1)$$

Where C_0 (μmol/L) represents the initial concentration of HRP solution, C_f (μmol/L) stands for the residue concentration of HRP, V (L) is the adsorption mixture volume, and m (g) is the quality of HMIPs.

2.5.2. Kinetics adsorption experiments

The HMIPs, HNIPs, SMIPs and SNIPs (10 mg) were mixed with 3 mL HRP solution (0.75 mg/mL) and kept for various time (5–85 min), respectively. Followed by separation, the residual HRP concentration was determined by UV spectrometer. The adsorption capacity (Q) of the HMIPs, HNIPs, SMIPs and SNIPs for HRP was calculated using formula (1), respectively.

2.5.3. Selectivity experiments

The selectivity of the HMIPs, HNIPs, SMIPs and SNIPs was evaluated using BSA, Hb, Cyt C, OVA and Lys as competitors. Imprinting factor (IF) was calculated using formula (2) to estimate the recognition capability.

$$IF = Q_{HMIPs}/Q_{HNIPs} \quad (2)$$

Where Q_{HMIPs} and Q_{HNIPs} represent the binding capacity of the imprinted polymers and non-imprinted polymers, respectively.

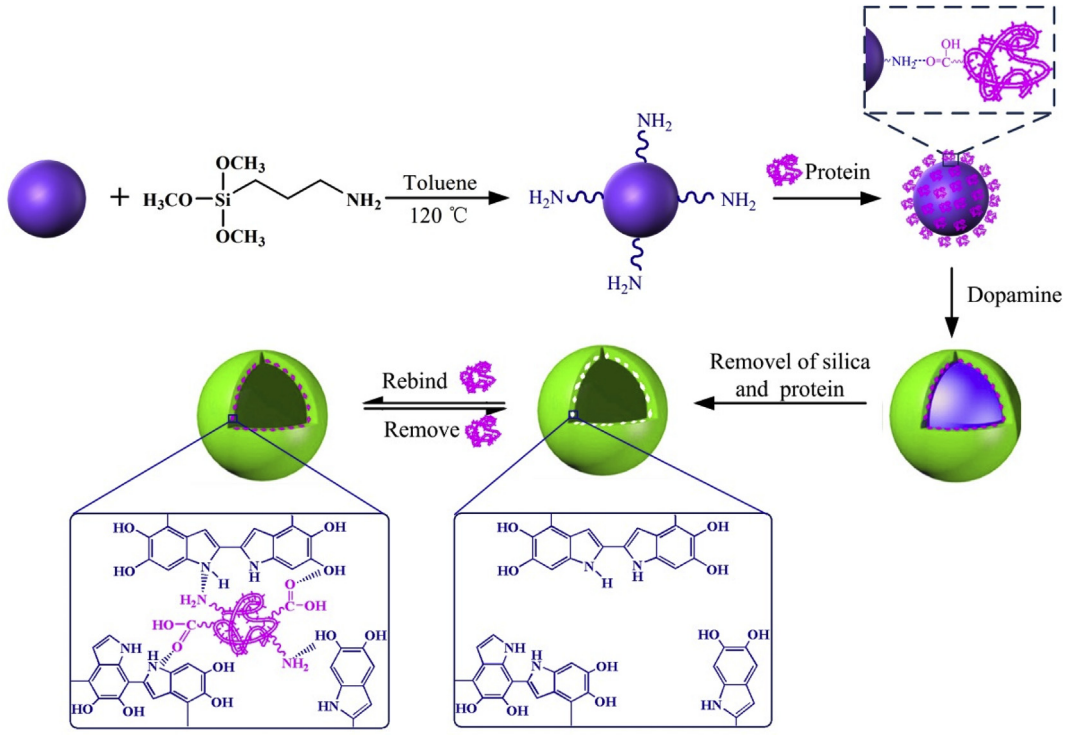

Fig. 1. Overall scheme for synthesis of HMIPs.

3. Results and discussion

3.1. Preparation of hollow molecularly imprinted polymers

The overall scheme for the synthesis of HMIPs was illustrated in Fig. 1. Firstly, uniform size and well dispersed SiO_2 were synthesized by Stöber method and used as sacrificial matrix to form hollow imprinted polymers. Sequentially, amino group as connecting group for target protein immobilization was grafted onto the SiO_2 surface, leading to amino functionalized SiO_2 (SiO_2@NH_2). In the next step, HRP was immobilized onto SiO_2@NH_2 surface through forming multi-hydrogen bonds interaction between amino groups and carboxyl group in protein (Gao et al., 2014; Zhang et al., 2018; Zhu et al., 2016), then an adherent multifunctional polydopamine layer was coated on the surface of SiO_2@NH_2-protein complex. Finally, the silica matrix and the embedded template protein were removed, generating HMIPs with binding sites corresponding to HRP in size, spatial structure and distribution of functional groups. As described by the reported literature, protein macromolecules could diffuse into the imprinted sites located in the polydopamine layer and can be easily washed out with acetic acid aqueous solution(Gao et al., 2014; Xia et al., 2013; Zhang et al., 2012; Zhu et al., 2016).

To ascertain the successful grafting of the amino functional groups on the surface of SiO_2, FT-IR spectra were used to characterize the chemical structure of SiO_2, SiO_2@NH_2, SMIPs and HMIPs. As shown in Fig. S1 (see Supporting Material), the infrared characteristic peaks of SiO_2 at 750 and 1102 cm^{-1} were ascribed to the stretching vibration of Si–O–Si. The adsorption peaks at 955 and 3312 cm^{-1} were attributed to the bending vibration of Si–OH and stretching vibration of –OH, respectively (Xia et al., 2013). While the FT-IR spectra of SiO_2@NH_2 displayed NH_2 peak at 1572 cm^{-1} and the relatively strong peak at 2954 cm^{-1} was the stretching vibration of C–H bonds ascribed to the methyl (or methylene) groups of APTES (Wang et al., 2012). Compared with SiO_2@NH_2, the new appearance of typical peaks in the spectra of SMIPs and HMIPs, phenylic C=C stretching at 1503 cm^{-1} and the enhanced adsorption peak intensity of C–N bond at 1621 cm^{-1} should be attributed to the coating of PDA layer on the SiO_2(Xia et al., 2013). While the fade adsorption peak of HMIPs at 1102 cm^{-1} confirmed the removal of SiO_2 core.

The adsorption capacity of SiO_2@NH_2 was investigated to confirm the successful immobilization of protein on the surface of SiO_2@NH_2. The amount of template protein ranged from 25 to 125 mg, while the amount of SiO_2@NH_2 maintained at a constant value of 200 mg. It can be seen in Fig. S2 that, the adsorption capacity of the SiO_2@NH_2 increased significantly with increasing the amount of HRP from 25 to 75 mg, and then maintained approximately constant from 75 to 125 mg. The results illustrated that the adsorption capacity of SiO_2@NH_2 were saturated over the 75 mg of HRP. Therefore, the template protein was successfully grafted on the surface of the SiO_2@NH_2.

The morphological structures of SiO_2, SMIPs and HMIPs were characterized by TEM as shown in Fig. 2. SiO_2 exhibited highly uniform spherical morphology. To calculate the size of the SiO_2, about 40 SiO_2 spheres shown in Fig. S3 were taken into account. The average diameter of the SiO_2 was 360 nm with standard deviations of ± 7.24 nm. TEM images of SMIPs showed that a thin semitransparent polymer layer was wrapped on the silica surface, while the HMIPs images demonstrated semitransparent cores, indicating the successful removal of silica matrix.

3.2. Optimization of the synthesis conditions

3.2.1. Effect of polydopamine layer thickness on imprinting factor

It has been reported that the imprinted layer thickness is critical to the binding properties of the imprinted material (Zhang et al., 2012). Herein, a series of SMIPs and HMIPs with uniform shell thickness were synthesized. As shown in Fig. S4, the thickness of the PDA shell can be modulated by changing the mass ratio of SiO_2@NH_2 and dopamine from 1/0.25, 1/0.5, 1/1, 1/2 to 1/4, corresponding to the imprinted PDA layer thickness of 8 nm (a, f), 16 nm (b, g), 25 nm (c, h), 33 nm (d, i) and 42 nm (e, j), respectively.

The effect of polydopamine shell thickness on the adsorption properties of the SMIPs and HMIPs was investigated. As shown in Fig.

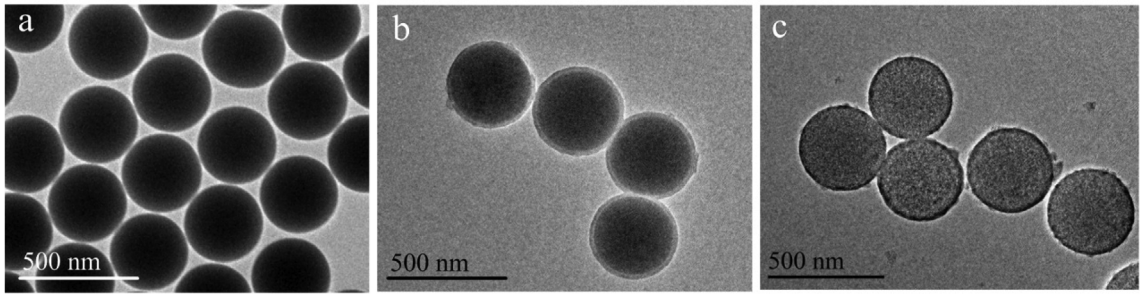

Fig. 2. TEM images of SiO_2(a), SMIPs(b) and HMIPs(c).

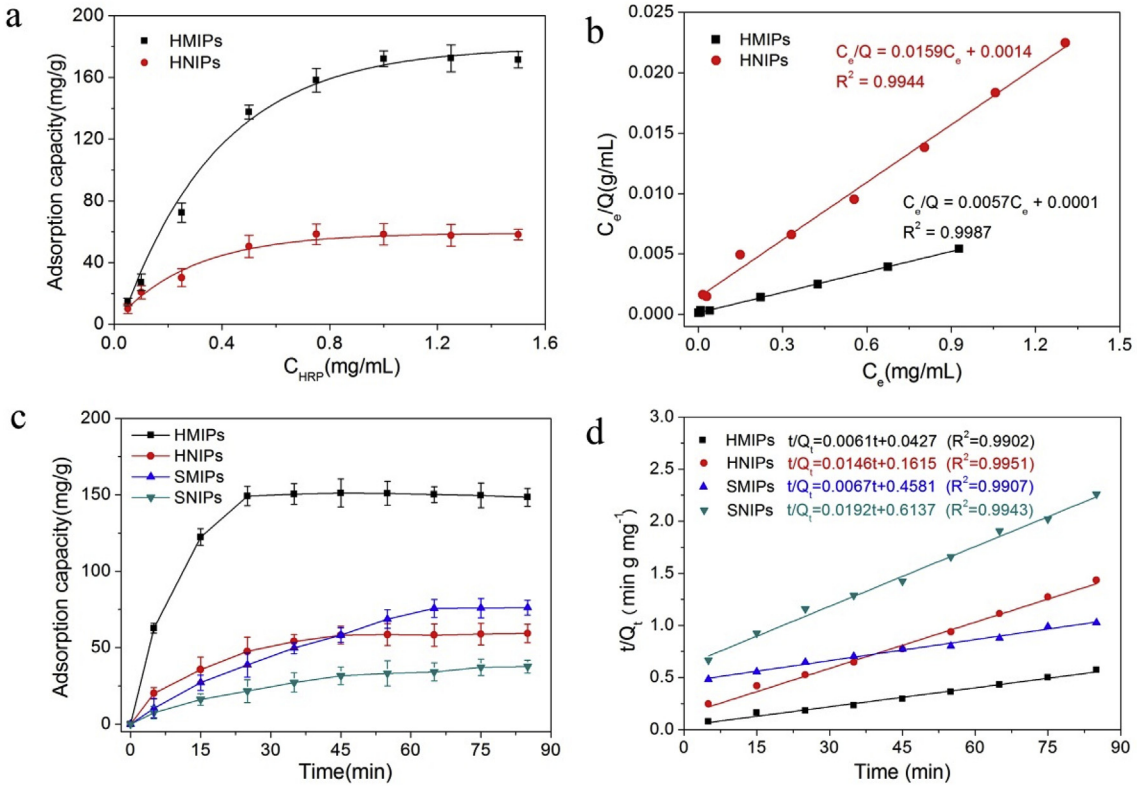

Fig. 3. (a) The adsorption isotherms of HRP onto HMIPs and HNIPs; (b) Scatchard plot of the adsorption assays of HRP on HMIPs and HNIPs; (c) The adsorption kinetics of HRP onto HMIPs, HNIPs, SMIPs and SNIPs; (d) Pesudo-second-order model to investigate the kinetic mechanism of HMIPs, HNIPs, SMIPs and SNIPs. The binding experiment was repeated for three times.

S5, the binding capacity of both SMIPs and HMIPs increased with the polydopamine shell thickness increased from 8 to 25 nm. Meanwhile, the imprinting factor of both SMIPs and HMIPs also increased as the increasing shell thickness. The weaker recognition capability of the thinner imprinted polymer layer suggested that only a part of template protein information was recorded during the imprinting process. However, both the binding capacity and the imprinting factor deteriorated with further increasing the polydopamine shell thickness from 25 to 42 nm, mainly due to the decreasing binding sites density in the imprinted materials. Moreover, the decrease in the binding capacity and imprinting factor of the thicker imprinted polymer layer may result from the larger mass transfer resistance. This result agreed well with the previous report (Hao et al., 2016; Qian et al., 2017; Zhang et al., 2012). The imprinting factor of the HMIPs was better than those of the SMIPs probably due to the template protein in the HMIPs were removed more thoroughly and more protein molecules could diffuse into the recognition sites.

3.2.2. Effect of template protein amount and polymerization time on binding capacity

The amount of template protein was another important factor which influenced the adsorption properties of the HMIPs. As shown in Fig. S6, the binding capacity of HMIPs increased obviously as the amount of template ranging from 25 to 75 mg, owing to a growing number of imprinting sites. Further increasing the amount of template, both binding capacity and imprinting factor decreased. This may result from the strong interaction among protein molecules, which led to aggregation of template molecules. The result demonstrated that the binding capacity of the HMIPs increased as with increasing imprinted molecules density in MIPs in a certain range, and then decreased with further increasing the imprinted molecules density in MIPs. This result agreed well with the previous report(Gao et al., 2014; Xia et al., 2013).

Sequentially, the amount of template was fixed at 75 mg, and the influence of the polymerization time on binding capacity was evaluated. As demonstrated in Fig. S7, the maximum adsorption capacity was obtained when the imprinting time was 9 h. The polymerization was uncompleted when the polymerization time was less than 9 h,

causing lower imprinting effect. The dopamine may self-polymerize and block the binding sites with further prolonging the polymerization time, worsening binding properties. Therefore, the optimal polymerization time was set to be 9 h.

3.3. Binding properties of HMIPs

3.3.1. Effect of pH on binding capacity of HMIPs

The effect of pH on the binding capacity of HMIPs was investigated. As shown in Fig. S8, the binding capacity of the HMIPs had no significant differences as changing the pH from 6.0 to 9.0. This phenomenon may be explained by the fact that the surrounding pH had negligible effect on the interactions between the HRP and multifunctional groups in the polydopamine layer. We chose pH 7.3 in this work because it was closed to the physiological pH, which would favor the selective enrichment of protein from real samples(Matsumoto et al., 2003; Zhu et al., 2018).

3.3.2. Adsorption isotherms

The saturation adsorption experiments were carried out at different HRP concentrations (0.05–1.5 mg/mL) to investigate the adsorption properties of HMIPs and HNIPs. It can be seen from Fig. 3a that, the binding capacity of HMIPs increased significantly with the increment of HRP concentrations, and then achieved equilibrium at 1.0 mg/mL. The maximum adsorption capacity of HMIPs and HNIPs were 172.1 mg/g and 58.3 mg/g, respectively. And the imprinting factor of HMIPs was 2.95 calculated by equation (2). It was obvious that the amount of HRP bound to the HMIPs was higher than that of HRP bound to the HNIPs, owing to the specific binding sites obtained in the polydopamine network. Unlike HMIPs, the binding of HNIPs was dominated by non-specific effect. To further investigate the binding properties of HMIPs and HNIPs, Langmuir isotherm model was used to describe the adsorption data, which can be expressed by formula (3):

$$\frac{C_e}{Q_e} = \frac{1}{K_m Q_m} + \frac{C_e}{Q_m} \tag{3}$$

where C_e (mg/mL) represents the equilibrium concentration of HRP in supernatant, Q_m (mL/mg) and K_m (mg/g) are the theoretical maximum binding capacity and Langmuir adsorption equilibrium constant, respectively (Hao et al., 2016). The satisfactory regression coefficients of HMIPs and HNIPs ($R^2 > 0.99$) in Fig. 3b indicated that the experimental data were consistent with the Langmuir adsorption isotherm. Afterwards, according to the slope and the intercept of the liner regression equations, the theoretical saturation adsorption capacity (Q_m) and Langmuir adsorption equilibrium constant (K_m) of HMIPs and HNIPs were calculated and listed in Table 1. As can be seen from Table 1, the K_m and Q_m of HMIPs (K_m: 57.00 mL/mg, Q_m: 175.44 mg/g) were significantly larger than those of HNIPs (K_m: 11.36 mL/mg, Q_m: 62.89 mg/g), indicating the existence of imprinted cavities in HMIPs (Gao et al., 2016; Li et al., 2016; Qian et al., 2017). Abundant functional groups presented on the polydopamine surface, and thus the adsorption of HRP on the HNIPs mainly originated from the non-specific binding. This was coincident with the theory that the corresponding MIPs can exhibit a significant imprinting effect only when NIPs show reasonable affinity toward a target molecule (Baggiani et al., 2012).

3.3.3. Adsorption kinetics

The adsorption kinetics of HRP on the imprinted materials was illustrated in Fig. 3c. It could be easy observed that the amount of HRP adsorbed on HMIPs and HNIPs shot up in the first 15 min, followed by gently increase until the adsorption equilibrium at 25 min. For the control experiment, the adsorption kinetics of HRP on SMIPs and SNIPs were also studied. However, more than 60 min were needed for the SMIPs to reach the adsorption equilibrium. The relative rapid adsorption rate of HMIPs was possibly due to the hollow structure. In this regard, more binding sites were located at the inner surface of the imprinted shells which was beneficial for the accessibility of HRP. It can be observed that the adsorption rate of the HMIPs was much larger than that of other protein-MIPs proposed previously (Hao et al., 2016; Ma et al., 2016). It was worth noting that the binding capacity of HMIPs was higher than that of the SMIPs, mainly due to the amount of binding sites per gram of HMIPs was much larger than that of SMIPs after removal of the SiO_2 core. Also, the hollow structure of HMIPs caused easy removal of the template protein, boosting the binding capacity. Moreover, the template protein could diffuse into the exposed recognition sites on the inner wall of the HMIPs owing to the hollow structure, further improving the binding capacity(Chen et al., 2013; Gong et al., 2016; Guan et al., 2007; Hua et al., 2018; Lu and Xu, 2017; Wang et al., 2016).

To further elucidate the mass transfer mechanisms of the binding process, the kinetic data were described by pseudo-second-order rate kinetic models which can be expressed by equation (4).

$$\frac{t}{Q_t} = \frac{1}{K_2 Q_e^2} + \frac{t}{Q_e} = \frac{1}{v_0} + \frac{t}{Q_e} \tag{4}$$

where Q_e and Q_t (mg g^{-1}) represent the amount of HRP adsorbed onto HMIPs or HNIPs (or SMIPs and SNIPs) at the equilibrium and time t, respectively. K_2 (g mg^{-1} min^{-1}) is the rate constant of pseudo-second-order adsorption. v_0 (mg g^{-1} min^{-1}) stands for the initial adsorption rate (Hao et al., 2016).

The related adsorption kinetics parameters were calculated by equation (4) and listed in Table 2. As shown in Fig. 3d, the pseudo-second-order model fit the experimental data quite well according to the high regression coefficients for each obtained materials ($R^2 > 0.99$). The v_0 of HMIPs (23.42 mg g^{-1} min^{-1}) was much higher than that of SMIPs (2.18 mg g^{-1} min^{-1}), suggesting that the adsorption of HRP on HMIPs was a fast process. It could be concluded that the hollow structure endowed the MIPs with both excellent binding capacity and satisfactory mass transfer rate.

3.3.4. Selectivity evaluation

According to the preparation process and the recognition mechanism of the imprinted polymers, the specific recognition sites located in the MIPs were complementary chemically and sterically to the target molecules (Baek et al., 2018; Bagheri et al., 2016a,b; Kryscio and Peppas, 2012; Liu et al., 2018). In this paper, to evaluate specificity of the HMIPs to HRP (Mw 44 kDa, pI 3.0–9.0), several proteins with different molecule weight and pI were chosen as interfering compounds. The molecule weight of BSA (Mw 66 kDa, pI 4.9) and Hb (Mw 64.5 kDa, pI 6.8–7.2) were higher than that of HRP, the molecule weight of Cyt C (Mw 12.7 kDa, pI 10) and Lys (Mw 14 kDa, pI 9.3) were lower than that of HRP, while OVA (Mw 45 kDa, pI 4.5) has similar molecule weight with HRP. In addition, these proteins had the different pI and structure which may verify the recognition sites were complementary to the

Table 1
The Langmuir adsorption constants for binding of HRP on HMIPs and HNIPs.

Sample	K_m (mL/mg)	Q_m (mg/g)	R^2
HMIPs	57.00	175.44	0.9987
HNIPs	11.36	62.89	0.9944

Table 2
Kinetic constants for the pseudo-second-order rate equations.

	K_2 (g $mg^{-1}min^{-1}$)	Q_e (mg g^{-1})	v_0 (mg g^{-1} min^{-1})	R^2
HMIPs	8.7×10^{-4}	163.93	23.42	0.9902
HNIPs	1.3×10^{-3}	68.49	6.19	0.9951
SMIPs	9.8×10^{-5}	149.25	2.18	0.9907
SNIPs	6.0×10^{-4}	52.08	1.62	0.9943

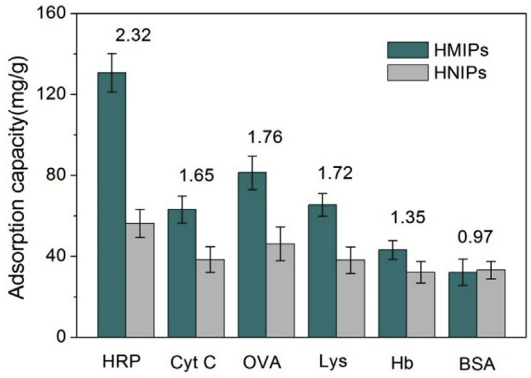

Fig. 4. The amounts of different proteins bound on HMIPs and HNIPs. The imprinting factors are displayed on the top of the column. Binding media: 20 mM PBS (pH 7.3); incubation time: 50 min; protein concentration: 0.5 mg/mL. The binding experiment was repeated for three times.

template protein. Fig. 4 displayed that the binding capacity and imprinting factor of HMIPs towards HRP were much higher than those of other protein, further confirming the existence of the imprinting sites. It was noteworthy that the binding capacity and imprinting factor of HMIPs for OVA was the second highest. That was probably because OVA possessed the similar molecular weight with HRP. This result indicated that the obtained HMIPs exhibited good specificity to the target protein.

3.3.5. Regeneration and application study

The HMIPs was further employed for selective separation of HRP from human serum sample. Human serum was chosen as real samples, because it was a complex biological sample, containing a great deal of proteins which may interfere the binding of the template protein. The human serum sample was diluted 50-fold with PBS (20 mM, pH 7.0) and spiked with 0.5 mg/mL HRP. Then the mixture was incubated with HMIPs for 50 min. As shown in Fig. S9, a noticeable peak was observed around 280 nm in the UV–vis spectrum of diluted human serum sample (Fig. S9a), indicating the existence of other constituent. When the human serum sample was spiked with HRP, the peak of HRP at 403 nm can be observed clearly (Fig. S9b), and HRP were detected in the elution after being incubated with HMIPs (Fig. S9c). However, no obvious peak around 403 nm was seen when the mixture was incubated with HNIPs (Fig. S9d). The results suggested the outstanding adsorption capacity and selectivity of the HMIPs and its potential in enriching HRP from a complex sample.

In order to evaluate the reusability of the HMIPs, we repeated the adsorption-desorption cycle four times. After the HRP adsorbed on HMIPs, the HMIPs was washed with 20% acetic acid/water (v/v) solution to remove the embedded template until no adsorption was detected by UV–vis spectrophotometer at about 280 nm. Then the recovered HMIPs was washed with PBS for several times, and reused for adsorption of HRP. As shown in Fig. S10, the HMIPs retained its adsorption capacity at 150 mg/g after four cycles of binding/removal, indicating the superior stability in the protein separation process.

3.3.6. Comparison

The adsorbing performance of the HMIPs was compared with other MIPs reported previously. As shown in Table S1, the adsorption capacity of the HMIPs was much higher than that of other protein imprinted polymers. And more remarkably, a faster mass transfer rate was obtained, which was superior to the reported MIPs. These results further proved the outstanding imprinting effect of the proposed strategy. However, the HMIPs exhibited lower imprinting factor than most of the MIPs, due to the multifunctional groups in the polydopamine network, which contributed to the binding of HRP on the HNIPs. Moreover, compared with the SMIPs, the binding capacity of the HNIPs was also improved after removal of the SiO_2 core, leading to the lower imprinting factor of the HMIPs.

4. Conclusions

In summary, hollow HRP-imprinted polymeric nanoparticle was prepared and used for HRP detection. The as-obtained HMIPs with controllable thickness exhibited excellent selectivity, reusability and stability. Moreover, the HMIPs could be used for enrichment of HRP from complex sample matrix, thus clearly indicating its great potential in the selective detection of proteins from real samples. Although the imprinting factor of the HMIPs was not prominent, we believe this strategy could promote the development of imprinting technology and adapt to the other macromolecules in future.

Declaration of interests

☒ The authors declare that they have no known competing financial interests or personal relationships that could have appeared to influence the work reported in this paper.

CRediT authorship contribution statement

Wei Chen: Conceptualization, Writing - original draft. **Min Fu:** Data curation. **Xixi Zhu:** Validation. **Qingyun Liu:** Writing - review & editing.

Acknowledgments

This work was supported by the Natural Science Foundation of Shandong Province (Grant No. ZR2018BB046, ZR2017BB008), National Natural Science Foundation of China (Grant No. 21805168), Scientific Research Foundation of Shandong University of Science and Technology for Recruited Talents (Grant No. 2017RCJJ040, 2017RCJJ041).

Appendix A. Supplementary data

Supplementary data to this article can be found online at https://doi.org/10.1016/j.bios.2019.111492.

References

Baek, I., Han, H., Baik, S., Helms, V., Kim, Y., 2018. Polymers 10 (9), 974.
Baggiani, C., Giovannoli, C., Anfossi, L., Passini, C., Baravalle, P., Giraudi, G., 2012. J. Am. Chem. Soc. 134 (3), 1513–1518.
Bagheri, H., Shirzadmehr, A., Rezaei, M., 2015. J. Mol. Liq. 212, 96–102.
Bagheri, H., Pajooheshpourb, N., Afkhamic, A., Khoshsafard, H., 2016a. RSC Adv. 6 (56), 51135–51145.
Bagheri, H., H.K, Amidi, S., Hosseinzadeh Ardakani, Y., 2016b. Anal. Methods 8, 3383–3390.
Chen, Y., He, X., Mao, J., Li, W., Zhang, Y., 2013. J. Sep. Sci. 36, 3449–3456.
Chen, W., Shea, K.J., Xue, M., Qiu, L., Lan, Y., Meng, Z., 2017. Anal. Bioanal. Chem. 409 (22), 5319–5326.
Dabrowski, M., Lach, P., Cieplak, M., Kutner, W., 2018. Biosens. Bioelectron. 102, 17–26.
Eersels, K., Lieberzeit, P., Wagner, P., 2016. ACS Sens. 1 (10), 1171–1187.
Gao, R., Zhang, L., Hao, Y., Cui, X., Tang, Y., 2014. RSC Adv. 4 (110), 64514–64524.
Gao, R., Hao, Y., Zhang, L., Cui, X., Liu, D., Zhang, M., Tang, Y., Zheng, Y., 2016. Chem. Eng. J. 284, 139–148.
Gong, C., Yang, Y., Yang, Y., Zheng, A., Liu, S., Tang, Q., 2016. J. Colloid Interface Sci. 481, 236–244.
Guan, G., Zhang, Z., Wang, Z., Liu, B., Gao, D., Xie, C., 2007. Adv. Mater. 19, 2370–2374.
Hao, Y., Gao, R., Liu, D., He, G., Tang, Y., Guo, Z., 2016. Talanta 153, 211–220.
Hua, S., Zhao, L., Cao, L., Wang, X., Gao, J., Xu, C., 2018. Chem. Eng. J. 345, 414–424.
Johari-Ahar, M., Karami, P., Ghanei, M., Afkhami, A., Bagheri, H., 2018. Biosens. Bioelectron. 107, 26–33.
Kryscio, D.R., Peppas, N.A., 2012. Acta Biomater. 8, 461–473.
Li, X., Zhou, J., Tian, L., Li, W., Ali, Z., Ali, N., Zhang, B., Zhang, H., Zhang, Q., 2016. Sens. Actuators, B 225, 436–445.
Liu, Y., Ai, K., Lu, L., 2014. Chem. Rev. 114 (9), 5057–5115.
Liu, S., Pan, J., Liu, J., Ma, Y., Qiu, F., Mei, L., Zeng, X., Pan, G., 2018. Small 14 (13),

1703968.
Lu, H., Xu, S., 2017. J. Chromatogr. A 1501, 10–17.
Lucci, P., Núnez, O., Galceran, M.T., 2011. J. Chromatogr. A 1218, 4828–4833.
Ma, R., Ha, W., Chen, J., Shi, Y., 2016. J. Mater. Chem. B 4 (15), 2620–2627.
Matsumoto, A., Ikeda, S., Harada, A., Kataoka, K., 2003. Biomacromolecules 4, 1410–1416.
Munawar, A., Tahir, M.A., Shaheen, A., Lieberzeit, P.A., Khan, W.S., Bajwa, S.Z., 2018. J. Hazard Mater. 342, 96–106.
Nakata, E., Nagase, T., Shinkai, S., Hamachi, I., 2004. J. Am. Chem. Soc. 126 (2), 490–495.
Nishino, H., Huang, C., Shea, K.J., 2006. Angew. Chem. Int. Ed. 45 (15), 2392–2396.
Pan, G., Sudhirkumar, Sing, S., Yeung, Y., Jakštaitė, M., Li, Q., Wingren, A.G., Sellergren, B., 2017. Angew. Chem. Int. Ed. 56 (50), 15959–15963.
Pan, J., Chen, W., Ma, Y., Pan, G., 2018. Chem. Soc. Rev. 47 (15), 5574–5587.
Pang, X., Cheng, G., Lu, S., Tang, E., 2006. Anal. Bioanal. Chem. 384 (1), 225–230.
Qian, L., Sun, J., Hou, C., Yang, J., Li, Y., Lei, D., Yang, M., Zhang, S., 2017. Talanta 168, 174–182.
Qiu, H., Pu, F., Ran, X., Liu, C., Ren, J., Qu, X., 2018. Anal. Chem. 90 (20), 11775–11779.
Saylan, Y., Akgonullu, S., Cimen, D., Derazshamshir, A., Bereli, N., Yilmaz, F., Denizli, A., 2017. Sens. Actuators, B 241, 446–454.
Uzun, L., Turner, A.P.F., 2016. Biosens. Bioelectron. 76, 131–144.
Wang, S., Wang, R., Wu, X., Wang, Y., Xue, C., Wu, J., Hong, J., Liu, J., Zhou, X., 2012. J. Chromatogr. B 905, 105–112.
Wang, J., Qiu, H., Shen, H., Pan, J., Dai, X., Yan, Y., Pan, G., Sellergren, B., 2016. Biosens. Bioelectron. 85, 387–394.
Xia, Z., Lin, Z., Xiao, Y., Wang, L., Zheng, J., Yang, H., Chen, G., 2013. Biosens. Bioelectron. 47, 120–126.
Xing, R., Wang, S., Bie, Z., He, H., Liu, Z., 2017. Nat. Protoc. 12 (5), 964–987.
Zeinali, S., Khoshsafar, H., Rezaei, M., Bagheri, H., 2018. Anal. Bioanal. Chem. Res. 5 (2), 195–204.
Zhang, M., Zhang, X., He, X., Chen, L., Zhang, Y., 2012. Nanoscale 4 (10), 3141–3147.
Zhang, Z., Wang, H., Wang, H., Wu, C., Li, M., Li, L., 2018. Analyst 143 (23), 5849–5856.
Zhu, X., Li, H., Liu, H., Peng, W., Zhong, S., Wang, Y., 2016. J. Sep. Sci. 39 (12), 2431–2437.
Zhu, H., Yao, H., Xia, K., Liu, J., Yin, X., Zhang, W., Pan, J., 2018. Chem. Eng. J. 346, 317–328.